ADVANCED FUNCTIONAL MATERIALS

DOI: 10.1002/adfm.200800640

Modifying Porous Silicon with Self-Assembled Monolayers for Biomedical Applications: The Influence of Surface Coverage on Stability and Biomolecule Coupling**

By *Till Böcking, Kristopher A. Kilian, Katharina Gaus,* and *J. Justin Gooding**

Integrating nanostructured silicon materials with aqueous biological systems requires a suitable chemical passivation that can be controlled in a reproducible fashion. Herein, we investigate in detail a facile method to control both the stability of a porous silicon rugate filter and the degree to which the material can be functionalized with biological molecules. Hydrosilylation of neat and dilute undecenoic acid over time leads to monolayers with different chemical surface coverage within the mesoporous architecture. We show how the shift in the reflectance spectrum, as a result of the change in the average refractive index of the rugate filter, can be used to assess the coverage of organic molecules on the pore surfaces. Surfaces with low monolayer coverage dissolve rapidly when exposed to aqueous solutions but are amenable to a high degree of biological functionalization. Surfaces with high coverage show exceptional stability but are biologically modified to a lesser degree. Therefore, tailoring the reaction conditions can be used to suit the application where control of stability and degree of biological modification are important criterion. Surfaces fabricated within the intermediate regime display both good stability and efficient biomolecule conjugation thus making them ideal for sensing applications. Biosensing utility is demonstrated by detecting active protease within the crystal by cleavage of immobilized peptides.

1. Introduction

Porous silicon (PSi) is a versatile material for optical devices owing to the ease and flexibility of its fabrication by anodization of single crystal silicon in HF containing electrolyte solutions. The pore size, geometry, and porosity of the material (i.e., the volume ratio of air to silicon) can readily be tuned by varying the doping type or level of the silicon substrate, the electrolyte composition, or etching conditions.[1] Importantly, the refractive index (n) of the material is determined by its porosity, which can be tuned precisely by controlling the current density during the electrochemical etching process. This ability to continuously tune the material's refractive index normal to the substrate surface opens the door to facile fabrication of one-dimensional photonic crystals such as Bragg reflectors,[2] resonant microcavities[3], and rugate filters.[4]

A wide range of biomedical applications including biosensing,[5–9] implantable devices[10,11], and drug delivery[12–15] have been developed on the basis of PSi, whereby the PSi thin film (usually with a thickness in the μm range) can remain attached to the silicon substrate for use as a sensor chip or it can be lifted off from its substrate and broken into micron sized PSi particles by sonication.[16] Biosensing with PSi relies on the principle that capture or removal of molecular species on the inside of the porous matrix results in changes of the effective refractive index of the material and hence a shift in its reflectance spectrum. Initially, a range of affinity biosensors relying on binding of analytes to receptors immobilized on the pore walls were developed.[5,9,17] A more recent focus has been on the use of PSi biosensors for monitoring enzymatic activity either by enzymes degrading a substrate that is coating the PSi optical filter[18] or is attached to its pore walls.[19] This latter strategy is exciting as it essentially exploits enzymatic amplification to give very sensitive biosensing structures (the lowest detected concentration of the protease enzyme subtilisin when degrading peptides attached to pore walls was 37 nM[19]). The interest in protease enzymes stems from protease activity being a marker of immune response and PSi being compatible with integration with cells to give a ''smart petri-dish''. This concept of a smart Petri-dish has been demonstrated in its simplest form for monitoring, in real-time, the viability of cells cultured on top of a modified PSi optical filter by changes in the scattering of light by the cell layer upon cell death.[20,21] Similarly, we have extended this concept to

[*] Prof. J. J. Gooding, Dr. T. Böcking, Dr. K. A. Kilian
School of Chemistry, University of New South Wales
Sydney 2052 (Australia)
E-mail: justin.gooding@unsw.edu.au
Dr. K. Gaus
Centre for Vascular Research, School of Medical Sciences
University of New South Wales, Sydney 2052 (Australia)

[**] This study was funded by the Australian Research Council. Supporting Information is available online from Wiley InterScience or from the author.

producing materials with dual functionalities by having different surface chemistries on the internal pore walls relative to the exterior surface. These dual function materials have applications for cell capture and sensing material released from these cells or targeted drug delivery.[22] Other novel applications of PSi particles beyond drug delivery have also been demonstrated, including self-orientating and assembling of PSi photonic crystals that sense their environment,[23,24] encoded particles for biomolecular screening[25] and particles with spectral barcodes.[26,27]

The key to exploit these materials for biomedical applications is surface chemistry. PSi must be chemically modified to stabilize the PSi matrix in aqueous environments. Furthermore, surface chemistry is required to introduce functional groups onto the pore walls and exterior surface of the PSi to enable the attachment of biomolecules. The stabilization is required as freshly prepared PSi is hydride-terminated and oxidizes rapidly in the presence of oxygen and water, eventually leading to dissolution of the structure. Since most PSi-based biosensors depend on changes in the effective refractive index of the material, oxidation is a major problem because it causes uncontrollable changes in the refractive index that can hinder the reliable detection of the analyte.[6] Even for applications that rely on dissolution for drug release[13] or as a means of signal transduction,[28] one needs to be able to control the dissolution rate of the material. Monolayer formation via hydrosilylation of unsaturated molecules (alkenes or alkynes) represents a convenient route for passivation of the PSi surfaces against degradation.[29] The modification of PSi with undecenoic acid at moderate temperatures ($\leq$120 °C)[30,31] or with microwave radiation[32] yields well-formed monolayers, whereby the molecules react exclusively via the double bond and not via the carboxylic acid group (as observed at high temperatures). The resulting carboxylic acid-terminated monolayers can then be further modified using standard solid-phase coupling techniques.

Despite the wealth of chemical modification explored for the PSi surface,[29] there are no studies that explore the optimal monolayer properties in the context of optical biosensors; in particular no studies have assessed the range of the surface coverage of the monolayer forming molecules on the PSi that can be achieved and how this impacts on the stability of the photonic crystals or the subsequent biofunctionalization of the PSi. An understanding of the optimal monolayer properties is vital for the use of PSi in biosensing in general, and for us to reach our goal of using PSi in cell-based chips in particular. Here, we report the extent that the surface coverage of monolayer forming molecules affects the stability, optical, and chemical properties of PSi-based rugate filters. Monolayers with low coverage can be readily activated and modified with biomolecules but do not confer sufficient protection against oxidation. When the monolayer coverage is high, the sample is well-passivated but no longer sufficiently reactive toward biomolecules. Thus, there is a balance between stabilization and degree to which the structure can be biofunctionalized. Depending on the application, this balance can be tuned by adjusting the level of the surface coverage.

2. Results and Discussion

2.1. Formation of Carboxylic Acid-Terminated Monolayers Inside Narrow Linewidth Porous Silicon Rugate Filters

Mesoporous silicon with a distribution of pore sizes between 4 and 40 nm was fabricated by electrochemical anodization of p-type Si (100) wafers in ethanolic HF solutions. During the etching process the current density was varied to produce an optical filter with a continuous (sinusoidal) variation of the porosity (and hence refractive index) perpendicular to the plane of the filter. The resulting rugate filter is a one-dimensional photonic crystal exhibiting a high reflectivity stop-band around a characteristic wavelength and low reflectivity elsewhere. We have shown in previous work that narrow linewidth stop-bands with a full-width half-maximum value of less than 15 nm can be produced when the index modulation is apodized (faded out) with a Gaussian envelope function and when refractive index matching layers at the air–PSi and PSi–Si interfaces are incorporated to compensate for the mismatch between the average index of the filter and the surrounding media.[4]

Freshly prepared hydride-terminated PSi rugate filters were functionalized with carboxylic acid-terminated monolayers by thermal hydrosilylation of 10-undecenoic acid. The extent of monolayer coverage was assessed by transmission FTIR spectroscopy. Reaction of a PSi rugate filter with 60 sinusoidal periods in neat 10-undecenoic acid for reaction times of up to 50 h resulted in only a low to medium yield of attached undecanoic acid chains as determined from the change in the Si–H_x band in the FTIR spectrum (see Supporting Information Fig. S1). Figure 1a shows the FTIR spectra of such a sample before and after monolayer formation. The Si–H_x ($x = 1, 2, 3$) stretches at ~2120 cm^{-1} of the freshly prepared PSi structure are consumed in the reaction with the alkene, and the peak area shows a decrease by just ~26% after the reaction (Fig. 1a, inset). In contrast, when the reaction was carried out in a solution of undecenoic acid in mesitylene, the PSi structure shows a high level of modification with a pronounced decrease in the Si–H_x peak area by ~50% (Fig. 1b, inset). Note that a 50% substitution of Si–H on a Si (111) surface would correspond to a complete monolayer coverage with this type of chemistry as the molecular footprint dictates that only every second Si–H bond can be replaced by an Si–C bond.[29] The difference in the degree of organic modification is also evident when comparing the intensities of the C–H (~2930 cm^{-1}) and C=O (~1716 cm^{-1}) stretching modes from the monolayer for the samples modified in neat and diluted undecenoic acid (Fig. 1a and b, respectively). Henceforth, we use the relative ratios of the peak intensities of the C=O to Si–H stretches as an indicator of surface coverage.

ADVANCED FUNCTIONAL MATERIALS

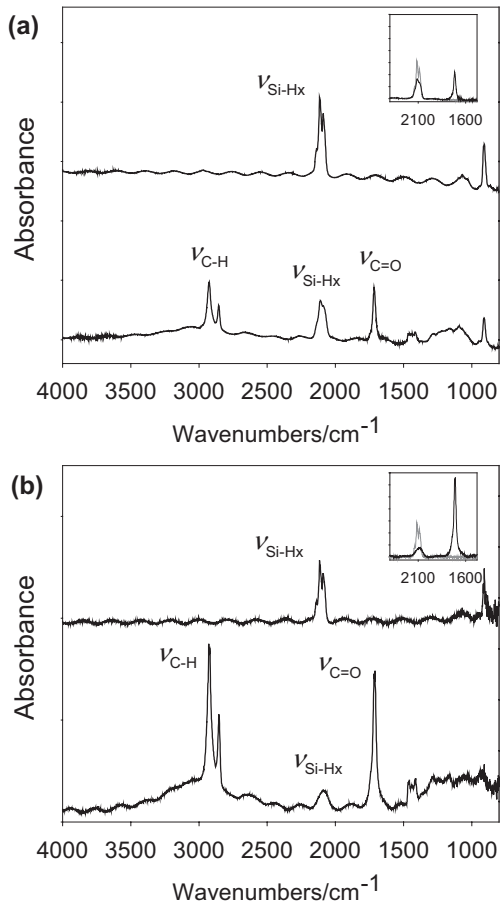

Figure 1. FTIR spectra of PSi rugate filters before and after monolayer formation for a sample modified a) with neat undecenoic acid for 50 h and b) with a solution of undecenoic acid in mesitylene for 20 h. The insets show an overlay of the region showing the Si–H_x stretches and C=O stretch of the respective set of spectra (after subtracting the interference fringe).

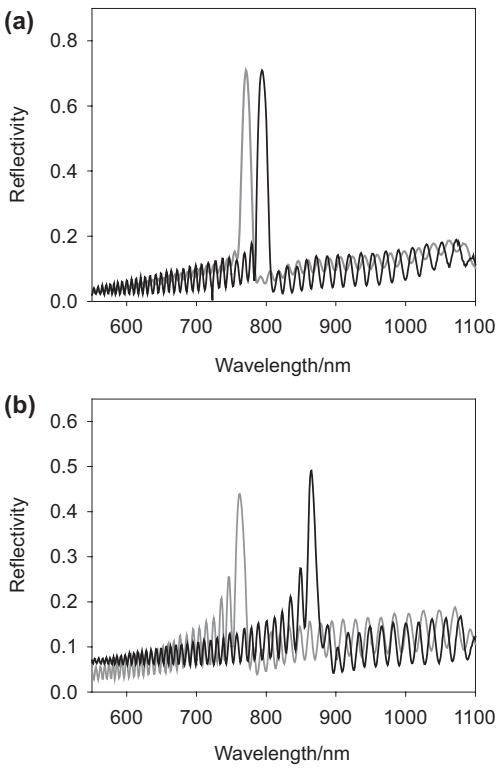

Figure 2. Reflectivity spectra of the same PSi rugate filters shown in Figure 1 before and after monolayer formation for a sample modified a) With neat undecenoic acid and b) a solution of undecenoic acid in mesitylene.

2.2. Optical Properties and Structural Integrity of Porous Silicon as a Function of Monolayer Surface Coverage

The alkylation of the PSi rugate filters is also evident from the changes of the optical properties of the filter because the spectral position of the stop-band depends on the effective refractive index of the filter. Upon monolayer formation, part of the air ($n = 1$) inside the pores is replaced with organic material ($n > 1$) resulting in a shift of the stop-band toward higher wavelengths. Figure 2 shows the optical reflectance spectra of the same samples analyzed by FTIR (shown in Fig. 1) before and after monolayer formation. As expected, the magnitude of the redshift of the stop-band was dependent on the level of alkylation; the filter with low monolayer coverage exhibits a shift of only 23 nm (Fig. 2a) whereas the stop-band of the filter with high monolayer coverage is shifted by 103 nm (Fig. 2b).

To further investigate the dependence of the optical properties of the filters on organic modification, we prepared over 50 PSi rugate filters with a wide range of monolayer coverages by reaction in neat or diluted undecenoic acid for varying periods of time. These modified filters were analyzed using FTIR and optical reflectance spectra to determine alkylation yield, level of oxide formation, and shift of the stop-band. To facilitate comparison between filters with a different number of periods, the ratio between the intensity of the carbonyl stretch to that of the residual Si–H_x stretch was used as a measure of monolayer coverage. All transmission FTIR spectra of PSi exhibit an interference fringe resulting from constructive and destructive interference of infrared light reflected at the air–PSi and PSi–Si interfaces; these fringes were subtracted (as shown in the insets of Fig. 1a and b) before determining the peak intensities. Figure 3 shows a plot of the redshift of the stop-band as a function of the $\nu_{C=O}/\nu_{Si-H_x}$ intensity ratio. The trend in the data confirms the expected relationship between the molecular coverage and the magnitude of the spectral shift of the stop-band, that is, the higher the level of alkylation as determined by FTIR, the higher the spectral redshift of the stop-band. Further, the shift of the stop-band is sensitive to side-reactions, such as oxidation, and its magnitude is generally consistent with incorporating species of different refractive index. The redshift is easily tuned by adjusting the length of the monolayer forming species (see Supporting Information Fig. S2–S4).

Importantly, the magnitude of the redshift of the stop-band is a reliable measure for the stability of the modified optical

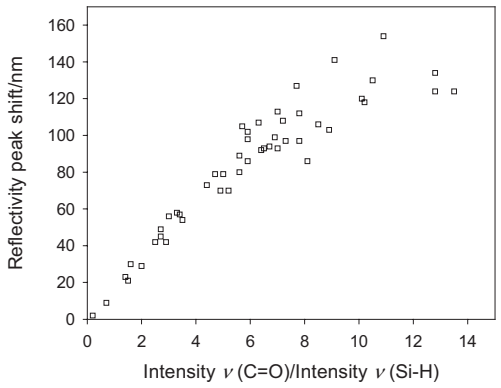

Figure 3. Shift of the high reflectivity peak after monolayer formation relative to the as prepared sample, as a function of the monolayer coverage expressed as a ratio of the intensity of the C=O stretch to that of the Si–H_x stretch.

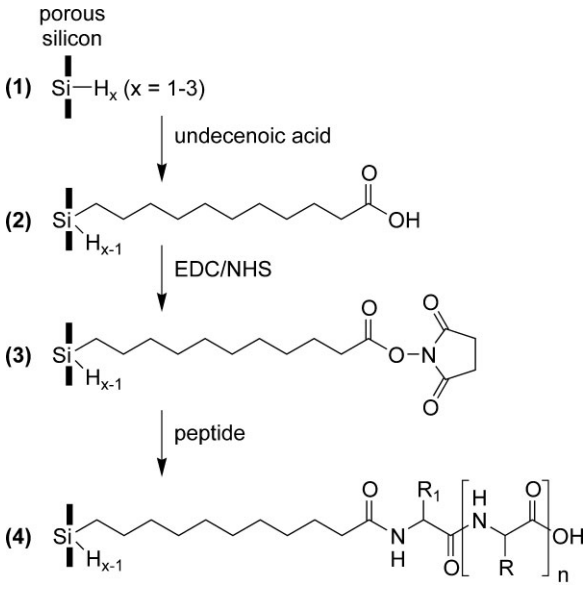

Scheme 1. Approach for biofunctionalization of PSi rugate filters.

filters in aqueous solutions. When samples with low surface coverage exhibiting a shift of less than 80 nm were immersed in aqueous buffers for 30 min, and subsequently rinsed with ethanol and blown dry under inert gas for inspection, varying degrees of structural collapse and disintegration of the porous matrix were apparent (Fig. 4a).[33] Concomitant with the loss of structural integrity, changes in the FTIR could be observed as discussed in more detail below. In contrast, samples with a shift of the stop-band above a threshold of 80 nm remained remarkably stable to chemical derivatization in aqueous environments (>24 h in aqueous protein solutions) without apparent structural collapse (Fig. 4b).

2.3. Biofunctionalization of Monolayer Modified Porous Silicon Rugate Filters Toward Sensing Applications

The chemical approach for attaching biomolecules to the PSi surfaces is shown in Scheme 1. After monolayer formation (surface 2), the PSi sample is treated with a solution of 1-ethyl-3-[3-dimethylaminopropyl]carbodiimide (EDC) and *N*-hydroxysuccinimide (NHS) to yield an activated monolayer (surface 3), which was reacted with a tripeptide (surface 4). The PSi optical filter was rinsed and dried after each modification step and inspected with FTIR and reflectance spectroscopy. We found striking differences in the resistance against oxidation, the structural stability, and the reactivity of the structures as a function of the monolayer coverage as discussed in the following sections for samples with low, intermediate, and high levels of alkylation. The physical properties of the samples used to illustrate these categories are summarized in Table 1.

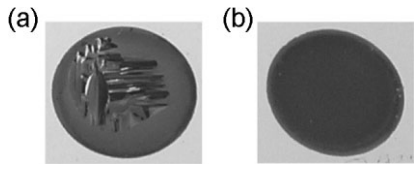

Figure 4. Photographs of PSi rugate filters modified with undecanoic acid monolayer with a) low coverage and b) high coverage after exposure to aqueous solutions.

2.3.1. Low Coverage Monolayers

Activation of PSi rugate filters with a low level of alkylation (redshift <80 nm) proceeds smoothly as apparent from the FTIR spectrum of such a sample ($\nu_{C=O}/\nu_{Si-H_x}$ intensity ratio of 2.5) after treatment with aqueous EDC/NHS (Fig. 5a, surface 3). The shift of the carbonyl stretch from 1714 cm^{-1} (characteristic of the free acid) to 1742 cm^{-1} along with the appearance of other absorbances characteristic of the NHS ester group (succinimidyl C=O groups at 1816 and 1787 cm^{-1}, N–O group at 1208 cm^{-1}, and C–O group at 1070 cm^{-1}) confirm a high level of activation. At the same time, the sample shows considerable levels of oxidation evident from appear-

Table 1. Summary of physical properties for samples with low, intermediate, and high monolayer coverage.

	Low	Intermediate	High
$I(\nu_{C=O})/I(\nu_{Si-H_x})$	2.5	7.0	10.9
Peak shift after SAM formation[b]	42 nm	112 nm	151 nm
Peak shift after peptide coupling[b]	N/A	53 nm	41 nm
EDC/NHS activation[a]	High	High	Low
Peptide coupling yield[a]	High	High	Low
Oxide formation[a]	High	Very low	Not detectable
Sample integrity	Collapsed	Intact	Intact

[a] FTIR data. [b] Reflectivity data.

ADVANCED FUNCTIONAL MATERIALS

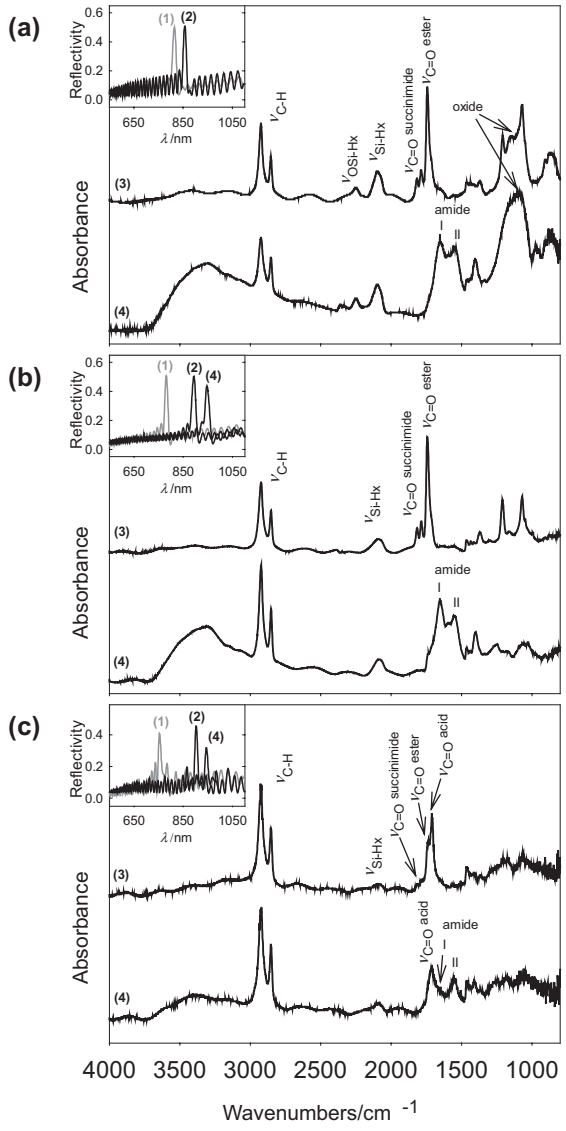

Figure 5. FTIR spectra of undecenoic acid modified PSi after activation of the carboxylic acid groups with EDC and NHS, and after coupling of a tripeptide to the activated monolayer for PSi samples with a) low surface coverage, b) medium to high surface coverage, and c) very high surface coverage. The insets show the optical reflectance spectra of the respective samples. The numbering of the spectra corresponds to the steps shown in Scheme 1: (1) as prepared (hydride-terminated), (2) after monolayer formation, (3) after activation with EDC/NHS, and (4) after coupling of a tripeptide.

ance of the Si–O–Si stretches at $\sim$1100 cm^{-1} and the OSi–H_x stretches at $\sim$2250 cm^{-1}, which appear due to migration of oxygen into the backbonds of the silicon lattice. The FTIR spectrum after peptide coupling (Fig. 5a, surface 4) clearly shows efficient aminolysis of the NHS esters by the tripeptide with the appearance of the amide I (C=O stretching) and amide II (N–H bending) bands at 1650 and 1545 cm^{-1}, respectively. The detachment of the PSi film off the Si substrate is also apparent from the disappearance of the interference fringe in the FTIR spectrum (Fig. 5a, surface 4). The dominant feature of the spectrum is the oxide peak revealing considerable increase in PSi oxidation during renewed exposure to aqueous buffers. A reflectivity spectrum could no longer be recorded on the filter after peptide coupling because the PSi thin film was partially lifted off the substrate. Thus, the collapse of the structure is presumably the result of oxidation and dissolution of the insufficiently passivated PSi matrix. We hypothesize that the strain created in the material due to uneven formation of oxide leads to the lift-off of the PSi layer from the substrate.

2.3.2. Intermediate Coverage Monolayers

PSi rugate filters with intermediate coverage monolayers also show high reactivity toward the activation of the carboxylic acid and subsequent coupling of peptides but without the problem of oxidation and structural collapse observed for samples with low monolayer coverage. The FTIR spectra of such a sample (Fig. 5b) clearly shows high yields of NHS ester formation (surface 2) followed by amide bond formation (surface 3) with very low signals attributable to Si–O–Si groups and no detectable signal for OSi–H_x groups. The reflectivity spectra show that the stop-band is shifted by 112 nm upon monolayer formation followed by a further 53 nm shift after immobilization of the tripeptide. The PSi layer remains intact, which is also apparent from the fact that the optical quality of the filter is maintained throughout the modification procedure and that the interference fringe in the FTIR spectra is maintained.

2.3.3. High Coverage Monolayers

Figure 5c shows the FTIR and reflectance spectra after successive modification steps for an optical filter with a high alkylation yield as characterized by a redshift of the stop-band by more than 120 nm. The sample shown as an example for this category exhibits a spectral shift of 151 nm upon monolayer formation (Fig. 5c, inset). Interestingly, the carboxylic acid-terminated layer cannot be efficiently activated. The FTIR spectrum of the filter after treatment with EDC and NHS (Fig. 5c, surface 3) shows a strong absorbance at 1712 cm^{-1}, characteristic of the carbonyl stretching of the free carboxylic acid group, whereas the signals assigned to the NHS ester and succinimidyl carbonyl stretches are comparatively weak. After reaction with the tripeptide, the FTIR spectrum (Fig. 5c, surface 4) exhibits a broad peak at 1712 cm^{-1} corresponding to the carbonyl stretch of the unreacted acid with a shoulder at $\sim$1650 cm^{-1} due to the presence of the amide I band. The amide II band is also present in the spectrum but considerably weaker than observed for the modified low and intermediate coverage samples. No oxidation of the structure is detectable and there are no observable cracks in the PSi thin film, i.e., structural integrity is maintained. Thus, PSi rugate filters with high coverage monolayers are highly passivated against

oxidation and dissolution but the majority of the carboxylic acid groups can no longer be efficiently modified using a standard solid phase coupling chemistry.

We attribute the steric hindrance arising from crowding of head groups at the top of the densely packed monolayer, especially when considering the additional constraints imposed by the pore geometry, as responsible for the poor chemical conversion. We also considered, but discounted, the possibility that the poor chemical conversion was due to blocking of the pores due to physisorption of contaminants as suggested previously for carboxylic acid-terminated monolayers.[34,35] The reason for discounting this possibility is a high coverage sample was rinsed with hot acetic acid, a procedure shown to remove physisorbed contaminants from undecanoic acid monolayers on flat Si.[35] There are no differences between the FTIR spectra before and after rinsing with hot acetic acid (see Supporting Information Fig. S4) suggesting that physisorption of unreacted undecenoic acid is not the cause for the lack of reactivity.

2.3.4. Protease Biosensor

Finally, we tested the stability of PSi rugate filers with intermediate coverage in a biosensing application, a demanding test because physisorption of proteins inside undecenoic acid modified PSi can lead to degradation and structural collapse. The optical filter was biofunctionalized with a decapeptide yielding a redshift of the stop-band by 21 nm (see Supporting Information Fig. S5). Exposure of the peptide chip to the protease subtilisin led to a blueshift of the stop-band by 6 nm, consistent with partial removal of the peptide from the pores as a result of degradation by the protease. Incubation in buffer on the other hand did not lead to a spectral shift of the stop-band. Importantly, the structure remained intact and there was no broadening of the stop-band (full-width half-maximum ~19 nm) throughout the biosensing experiment, indicating that the optical properties of the PSi optical filter were not affected.

3. Conclusions

The level of alkylation determines the material properties of PSi rugate filters. Low coverage monolayers can be readily biofunctionalized but do not offer long-term stabilization in aqueous environments. While material modified in this regime will cause unwanted signal drift in biosensing, it may be suitable and in many cases, preferable for drug delivery applications where tailoring the dissolution of non-toxic PSi in vivo is a desired criteria. For biosensing a higher level of alkylation is required to impart the desired resistance against collapse and disintegration. However, we found that when the alkylation level becomes too high the samples are no longer reactive toward further modification. Again, these samples with high coverage may prove beneficial for drug delivery applications where a small molecule therapeutic can be incorporated into the modified material with a prolonged in vivo dissolution time. For biosensing applications, intermediate amounts of alkylation is desired as it readily allows solid-phase coupling of biorecognition elements whilst resisting aqueous degradation over time. Fortunately, the magnitude of the redshift of the stop-band after monolayer formation can be used as a convenient measure to assess the extent of modification and the suitability of the modified filter for the intended application.

4. Experimental

Materials: All chemicals were obtained from Sigma–Aldrich and were of reagent grade or higher. 10-Undecenoic acid was redistilled under reduced pressure and stored under an inert atmosphere. 3-Butenoic acid was redistilled and stored under an inert atmosphere. Mesitylene was redistilled under reduced pressure from sodium and stored over molecular sieves under an inert atmosphere. Si (100) wafers (B-doped with a nominal resistivity of 0.07 Ω cm) were purchased from the Institute of Electronics Materials Technology (ITME).

Fabrication of Porous Silicon Rugate Filters: Si wafer pieces were cleaned by sonication in ethanol and acetone, blown dry under a stream of inert gas, and anodically etched in an electrochemical cell with a polished stainless steel disk as back contact and a platinum counter electrode using ethanolic HF (50% HF/100% ethanol, 1:1 v/v) as the electrolyte solution. The current density applied to the wafer was computer-controlled to obtain a sinusoidal index profile with apodization and refractive index matching layers at the air–PSi and PSi–Si interfaces. Typically, the rugate filters had 40–60 periods with a nominal sinusoidal porosity variation between 54 and 58% or 54.5 and 57.5%. Pauses in the etching program were incorporated to allow recovery of electrolyte concentration at the dissolution front. After etching the sample was rinsed with ethanol followed by pentane and blown dry under a stream of inert gas.

Monolayer Formation: Freshly prepared PSi rugate filters were modified by thermal hydrosilylation of 10-undecenoic acid or 3-butenoic acid inside customized Schlenk flasks with a flattened tube section to allow the PSi sample to be vertically immersed in a minimal volume of the reaction solution. The flame-dried flask was charged with the neat alkene or a solution of the alkene in mesitylene (1:2 v/v), and the liquid was degassed by four freeze-pump-thaw cycles before the PSi rugate filter was immersed under a flow of argon. The flask was then immersed in an oil bath at 120 °C and the reaction was allowed to proceed for 12–50 h. Finally, the sample was rinsed thoroughly with dichloromethane and ethyl acetate, and blown dry under a gentle stream of argon.

Monolayer Activation and Coupling of Peptides: PSi rugate filters modified with carboxylic acid-terminated monolayers were rinsed with ethanol to ensure wetting of the entire structure, then rinsed with water. Formation of NHS esters was achieved by immersing the wet sample in a solution of 0.1 M EDC and 0.1 M NHS for 1 h at room temperature. Immobilization of peptides via aminolysis of the reactive NHS esters was carried out by incubation of the wet sample in a solution of the peptide in phosphate buffered saline at pH 7.4. For analysis after each modification step, the sample was rinsed with water, ethanol, and dried under a gentle stream of argon.

Enzyme Experiment: PSi surfaces modified with the decapeptide Asp-Arg-Val-Tyr-Ile-His-Pro-Phe-His-Leu were placed in a glass vial with 1 mg mL^{-1} subtilisin in phosphate buffered saline for 4 h at 37 °C. Samples were then soaked in elution buffer [(1× SSPE) containing 1% 2-mercaptoethanol (v/v), 1% Triton X-100 (v/v)] for approximately 4 h, rinsed with 37 °C MilliQ water followed by 100% ethanol, dried under a stream of argon, and the reflectivity spectrum measured.

ADVANCED FUNCTIONAL MATERIALS

Spectroscopy: Transmission mode FTIR spectra were collected using ThermoNicolet AVATAR 370-FTIR spectrometer. Reflectivity spectra were measured at normal incidence over an area of 0.5 mm^2 by focusing monochromated light (J/Y SPEX 1681 spectrometer) onto the PSi sample and measuring the reflected light with a silicon detector.

Received: May 8, 2008
Revised: July 2, 2008
Published online: November 10, 2008

[1] H. Foell, M. Christophersen, J. Carstensen, G. Hasse, *Mater. Sci. Eng. R* **2002**, *R39*, 93.
[2] A. Bruyant, G. Lerondel, P. J. Reece, M. Gal, *Appl. Phys. Lett.* **2003**, *82*, 3227.
[3] P. J. Reece, G. Lerondel, W. H. Zheng, M. Gal, *Appl. Phys. Lett.* **2002**, *81*, 4895.
[4] S. Ilyas, T. Böcking, K. Kilian, P. J. Reece, J. Gooding, K. Gaus, M. Gal, *Opt. Mater.* **2007**, *29*, 619.
[5] V. S. Y. Lin, K. Motesharei, K.-P. S. Dancil, M. J. Sailor, M. R. Ghadiri, *Science* **1997**, *278*, 840.
[6] A. Janshoff, K.-P. S. Dancil, C. Steinem, D. P. Greiner, V. S. Y. Lin, C. Gurtner, K. Motesharei, M. J. Sailor, M. R. Ghadiri, *J. Am. Chem. Soc.* **1998**, *120*, 12108.
[7] C. Pacholski, M. Sartor, M. J. Sailor, F. Cunin, G. M. Miskelly, *J. Am. Chem. Soc.* **2005**, *127*, 11636.
[8] L. A. DeLouise, B. L. Miller, *Anal. Chem.* **2005**, *77*, **1950**.
[9] H. Ouyang, M. Christophersen, R. Viard, B. L. Miller, P. M. Fauchet, *Adv. Funct. Mater.* **2005**, *15*, 1851.
[10] K. A. Kilian, T. Böcking, K. Gaus, M. Gal, J. J. Gooding, *Biomaterials* **2007**, *28*, 3055.
[11] K. A. Kilian, T. Böcking, S. Ilyas, K. Gaus, W. Jessup, M. Gal, J. J. Gooding, *Adv. Funct. Mater.* **2007**, *17*, 2884.
[12] A. P. Loren, C. Pacholski, Y. L. Yang, S. V. Michael, J. S. Michael, *Nanomedicine* **2008**, *3*, 31.
[13] E. J. Anglin, M. P. Schwartz, V. P. Ng, L. A. Perelman, M. J. Sailor, *Langmuir* **2004**, *20*, 11264.
[14] J. L. Coffer, X. Li, J. St, John, R. F. Pinizzotto, Y. Chen, J. Newey, L. T. Canham, *Mater. Res. Soc. Symp. Proc.* **2000**, *599*, 61.
[15] F. Cunin, Y. Y. Li, M. J. Sailor, *BioMEMS Biomed. Nanotechnol.* **2006**, *3*, 213.
[16] J. L. Heinrich, C. L. Curtis, G. M. Credo, K. L. Kavanagh, M. J. Sailor, *Science* **1992**, *255*, 66.
[17] H. Ouyang, L. A. DeLouise, B. L. Miller, P. M. Fauchet, *Anal. Chem.* **2007**, *79*, 1502.
[18] M. M. Orosco, C. Pacholski, G. M. Miskelly, M. J. Sailor, *Adv. Mater.* **2006**, *18*, 1393.
[19] K. A. Kilian, T. Böcking, K. Gaus, M. Gal, J. J. Gooding, *ACS Nano.* **2007**, *1*, 355.
[20] M. P. Schwartz, A. M. Derfus, S. D. Alvarez, S. N. Bhatia, M. J. Sailor, *Langmuir* **2006**, *22*, 7084.
[21] S. D. Alvarez, M. P. Schwartz, B. Migliori, C. U. Rang, L. Chao, M. J. Sailor, *Phys. Status Solidi A* **2007**, *204*, 1439.
[22] K. A. Kilian, T. Böcking, K. Gaus, J. J. Gooding, *Angew. Chem. Int. Ed.* **2008**, *47*, 2697.
[23] J. R. Link, M. J. Sailor, *Proc. Natl. Acad. Sci. USA* **2003**, *100*, 10607.
[24] M. J. Sailor, J. R. Link, *Chem. Commun. (Cambridge, UK)* **2005**, 1375.
[25] F. Cunin, T. A. Schmedake, J. R. Link, Y. Y. Li, J. Koh, S. N. Bhatia, M. J. Sailor, *Nat. Mater.* **2002**, *1*, 39.
[26] S. O. Meade, M. S. Yoon, K. H. Ahn, M. J. Sailor, *Adv. Mater.* **2004**, *16*, 1811.
[27] S. O. Meade, M. J. Sailor, *Phys. Status Solidi RRL* **2007**, *1*, R71.
[28] C. Steinem, A. Janshoff, V. S. Y. Lin, N. H. Voelcker, M. R. Ghadiri, *Tetrahedron* **2004**, *60*, 11259.
[29] J. M. Buriak, *Chem. Rev.* **2002**, *102*, 1271.
[30] R. Boukherroub, D. D. M. Wayner, D. J. Lockwood, L. T. Canham, *Proc. Electrochem. Soc.* **2001**, 2001. 117.
[31] R. Boukherroub, A. Petit, A. Loupy, J.-N. Chazalviel, F. Ozanam, *J. Phys. Chem. B* **2003**, *107*, 13459.
[32] R. Boukherroub, J. T. C. Wojtyk, D. D. M. Wayner, D. J. Lockwood, *J. Electrochem. Soc.* **2002**, *149*, H59.
[33] L. Tay, N. L. Rowell, D. Poitras, J. W. Fraser, D. J. Lockwood, R. Boukherroub, *Can. J. Chem.* **2004**, *82*, 1545.
[34] A. Faucheux, A. C. Gouget-Laemmel, C. Douarche, C. H. de Villeneuve, F. Ozanam, P. Allongue, J. N. Chazalviel, R. Boukherroub, *Proc. Electrochem. Soc.* **2005**, 2005. 188.
[35] A. Faucheux, A. C. Gouget-Laemmel, C. Henry de Villeneuve, R. Boukherroub, F. Ozanam, P. Allongue, J.-N. Chazalviel, *Langmuir* **2006**, *22*, 153.